Journal of Hydroscience and Hydraulic Engineering
Vol.21, No.1 May, 2003, 23-40

GENERATION PROCESS OF ALTERNATE BAR UNDER UNSTEADY FLOW CONDITIONS

By

Yasuharu Watanabe
Civil Engineering Research Institute, Sapporo, Japan

Koji Sato
Asahikawa D. C. Department, Ministry of Land, Infrastructure and Transport, Asahikawa, Japan

and

Fumiaki Oyama
Abashiri branch office, Hokkaisuiko Consultant Corporation, Abashiri, Japan

SYNOPSIS

In our previous research on sand bed stability with finite amplitude and growth of alternate bars (1, 8), it is assumed that flow discharge is constant. Hydraulic experiments on the formation of alternate bars under unsteady flow conditions were conducted. Results of experiments suggested that finite amplitude effects of the flood-wave on alternate bar formation were not negligible when investigating their behavior under unsteady flow conditions. The wavelength and wave height of alternate bars differ significantly between unsteady and steady flow conditions and between rising and falling stage of the water level due to the flood wave. Liner stability analysis under unsteady flow conditions is applied to results of the experiments. The time variable basic state of flow is used in this analysis. Findings indicate that the analysis expresses the characteristics of bar generation process under unsteady flow conditions. The applicability of the analysis is also investigated in this paper.

INTRODUCTION

In alluvial rivers, alternate bars cause the channel to meander, as well as local aggregation and scouring, inducing river disaster. On the other hand, riffles and pools formed by bars are good habitats for aquatic organisms. Since the behavior of alternate bars must be fully understood for river planning, river structure layout, and the like. Numerous river engineering studies on bar formation have been conducted for disaster prevention and river environments. The river flow was assumed to be steady in these studies. This was based on the hypothesis that the time required for sandbar formation is extremely long as compared with the rate of change in flow. In general, bed form changes during flood time. It is necessary to clarify the effects of unsteady flow condition on bar generation

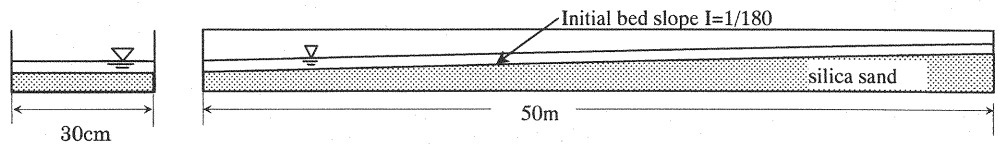

Figure 1 Experimental channel

Table 1 Hydraulic conditions and experimental results of steady flow experiments

Run	$2\tilde{B}$ cm	$\tilde{Q}$ cm^3/s	$\tilde{D}$ cm	$\tilde{T}$ min.	I_w	I_b	C_f	β	$1/d_s$	ϑ	Bars*	$\tilde{L}_b$ m	$\tilde{Z}_{bobs}$ cm	λ	Z_{bobs}
S-1	30	750	1.02	300	1/179	-	0.0093	14.7	13.4	0.045	A	3.4	3.4	0.28	3.33
S-2	30	1320	1.49	255	1/180	-	0.0093	10.1	19.6	0.066	A	3.1	2.1	0.30	1.41
S-3	30	1990	1.95	225	1/179	-	0.0092	7.7	25.7	0.087	A	2.0	2.5	0.47	1.28
S-4	30	2500	2.32	285	1/182	-	0.0097	6.5	30.5	0.102	A	2.1	2.5	0.45	0.08
S-5	30	3070	2.66	210	1/182	-	0.0097	5.6	35.0	0.117	N	-	-	-	-
S-6	30	3470	2.92	210	1/180	-	0.0101	5.1	38.4	0.129	N	-	-	-	-

*A=Alternate bars; and N=No bars.

process.

Tubino (6) conducted non-linear analysis of the critical region of sandbar formation, to clarify sandbar behavior under unsteady flow. Miwa et al. (5) performed a hydraulic experiment in order to analyze sandbar behavior with respect to discharge. The results of these studies revealed the significance of unsteady flow in sandbar formation. Investigations assumed a maximum discharge twice the minimum under unsteady flow. Regarding floods in Japan, the assumed value of maximum discharges must be increased.

In this study, the hydraulic experiments on the formation process of alternate bars were conducted. The results were compared with linear stability analysis proposed by Watanabe et al. (9). The aim of this research is to corroborate the differences between sand bar formations under steady and unsteady flow.

HYDRAULIC EXPERIMENTS ON BAR FORMATION (10)

Hydraulic experiments were conducted to determine the difference of bar development process under steady and unsteady flow conditions. An experimental channel with a length of 50m and a width of 0.3m was used. The channel bed composed of silica sand with a diameter of 0.76mm at a slope of 1/180. Figure 1 shows the sketch of the experimental flume.

Steady Flow Experiments

Experiments under steady flow conditions were conducted to reconfirm the bar development processes under steady flow. The water depth of experiments $\tilde{D}$ was set at 1 to 3cm considering the generating condition of alternate bars. The hydraulic conditions of steady flow experiments and the results were summarized in Table 1. Here, $2\tilde{B}$ = channel width; $\tilde{Q}$ = discharge; $\tilde{T}$ = elapsed time of water flow; I_w = water surface gradient; I_b = bed slope; C_f = frictional coefficient; β = channel width to depth ratio; d_s = dimensionless grain diameter ($=\tilde{d}_s/\tilde{D}$); ϑ = Shields parameter; λ = bar wave number ($=2\pi\tilde{B}/\tilde{L}_b$); $\tilde{L}_b$ = bar wavelength; Z_{bobs} = dimensionless

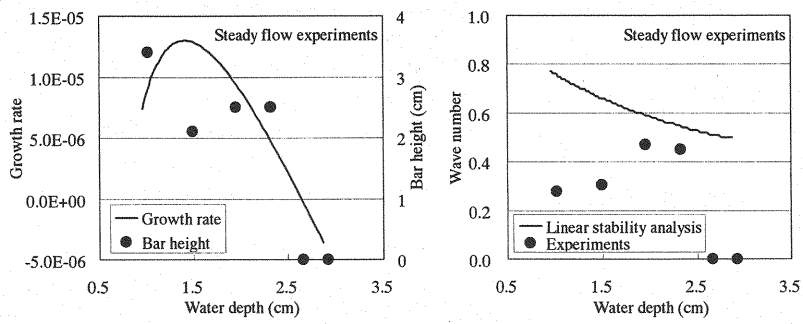

Figure 2 Comparison of the experimental results with theoretical results

bar height ($=\tilde{Z}_{bobs}/\tilde{D}$); and $\tilde{Z}_{bobs}$ = experimental result of bar height. Alternate bars formed in all runs except for runs S-5 and S-6. In these experimental cases, fully developed sandbars appeared after 200 to 250 minutes of water flow. Thereafter, the sandbar wave height and wavelength did not change over time.

Experimental results under steady flow conditions were compared with the linear stability analysis that was proposed by Colombini et al. (1) in Figure 2. The growth rate of bars by the linear stability analysis produced a negative value in the case where water depth was greater than 2.6cm and the experimental results show no bars in these conditions (runs S-5 and S-6). The linear stability analysis cannot treat bar height. However, some relation was observed between bar growth rate of linear stability analysis and observed bar height. The estimated wave number of bars, however, was greater than the experimental result. The estimated wave number doubled that of the experimental one in runs S-1 and S-2 which were small water depth. The linear stability analysis failed to reproduce the phenomenon that two pairs of alternate bars became a single pair. It is shown that the linear stability analysis can mostly express bar behaviors, especially bar generations under steady flow conditions.

Unsteady Flow Experiments

Three cases of unsteady flow experiment were conducted. The bed material was the same as that used in the steady flow experiments. The hydrograph of the unsteady flow experiments was selected in consideration of flood waveforms in actual rivers. Hasegawa (3) expressed the waveform of 1981 snow melting flood at an observation point that is 15km upstream from the Shiribetsu River Mouth as Equation (1). Equation (1) is used in runs U-1 and U-2. In these cases, initial water depth (depth of base flow) $\tilde{D}_B$ and the water depth at the end of hydrograph were set 1cm so that Shields parameter might be a critical shear stress ϑ_c. The maximum water depth $\tilde{D}_P$ was set at approximately 3 times of initial water depth, considering that alternate bars did not form when the water depth was greater than 2.7cm in the steady flow experiments.

$$D_0 = \left[\frac{\delta_f(\tau+\alpha_f)^2}{\tau^2+\beta_f} - \gamma_f\right]^{\frac{3}{2}} \tag{1}$$

where $D_0 = \tilde{D}_0/\tilde{D}_B$; $\tilde{D}_0$ = water depth by flood wave; $\tau = \tilde{t}\tilde{\sigma}$; $\tilde{t}$ = time; $1/\tilde{\sigma}$ = duration of flood (hydrograph). In order for the maximum water depth to occur at $\tau = 0.25$, parameters were set as $\alpha_f = 0.522$, $\beta_f = 0.131$, $\gamma_f = 1.15$ and $\delta_f = 1.03$. The flood duration of run U-1 was 8 hours, which is approximately twice the time taken for sandbar

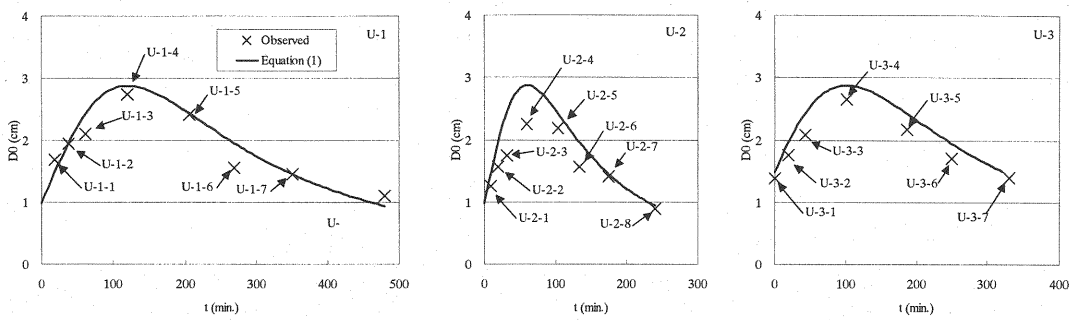

Figure 3 The time dependence of water depth and observed stage in runs U-1, U-2 and U-3

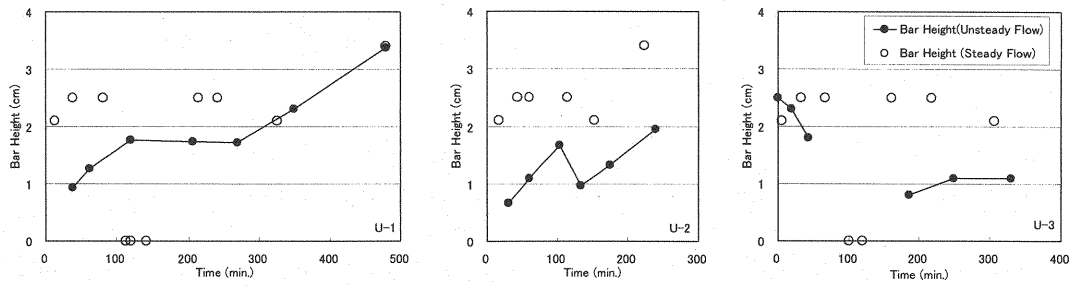

Figure 4 Bar height in experiments

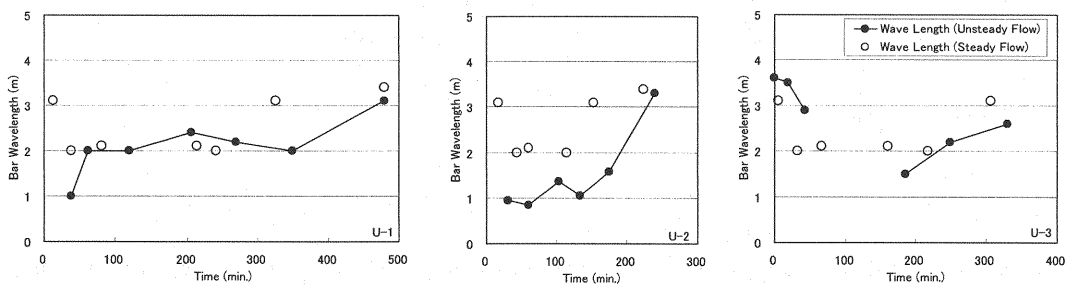

Figure 5 Bar wavelength in experiments

formation in the steady flow experiments. The flood duration of run U-2 was 4 hours, which is about the same as the time taken for sandbar formation in the steady flow experiments. To determine the changes of sandbars under the unsteady flow, the bed configurations were observed at 8 stages of the hydrograph in each case. Water flow was stopped for taking measurements of bed configuration because instruments could not function in the presence of water. Since the study aimed to clarify the behavior of sandbars over time under unsteady flow, the original state of the riverbed was recreated and water flowed from the beginning of hydrograph for each measurement of bed configuration. The times at which the bed configurations were measured were 19, 38, 62, 120, 206, 269, 350 and 480 minutes in run U-1, and 9, 19, 31, 60, 103, 134, 175 and 240 minutes in run U-2. The time dependence of depth in runs U-1 and U-2, and the observed time are shown in Figure 3.

On the other hand, run U-3 was performed in order to determine the influence of initial bed configuration on bar formation under the unsteady flow. Alternate bars formed by steady flow whose depth was about 1.5cm were used

Table 2 Hydraulic conditions and experimental results of unsteady flow experiments

Run	$2\tilde{B}$ cm	$\tilde{Q}$ cm^3/s	$\tilde{D}$ cm	$\tilde{T}$ min.	I_w	I_b	C_f	β	$1/d_s$	ϑ	Bar s	$\tilde{L}_b$ m	$\tilde{Z}_{bobs}$ cm	λ	Z_{bobs}
U-1-1	30	1330	1.69	19	1/185	1/179	0.0130	8.9	22.2	0.073	N	-	-	-	-
U-1-2	30	2030	1.95	38	1/182	1/181	0.0087	7.7	25.7	0.085	A	1.0	0.9	0.94	0.48
U-1-3	30	2910	2.10	62	1/168	1/180	0.0057	7.1	27.6	0.100	A	2.0	1.3	0.47	0.60
U-1-4	30	3840	2.74	120	1/204	1/177	0.0060	5.5	36.1	0.107	A	2.0	1.8	0.47	0.64
U-1-5	30	2890	2.42	206	1/174	1/176	0.0086	6.2	31.8	0.111	A	2.4	1.7	0.39	0.72
U-1-6	30	2070	1.56	269	1/175	1/180	0.0045	9.6	20.5	0.071	A	2.2	1.7	0.43	1.10
U-1-7	30	1330	1.46	350	1/166	1/177	0.0093	10.3	19.2	0.070	A	2.0	2.3	0.47	1.58
U-1-8	30	750	1.11	480	1/176	1/176	0.0122	13.5	14.6	0.050	A	3.1	3.4	0.30	3.04
U-2-1	30	1330	1.25	9	1/177	1/174	0.0055	12.0	16.4	0.056	N	-	-	-	-
U-2-2	30	2030	1.57	19	1/200	1/176	0.0041	9.6	20.7	0.063	N	-	-	-	-
U-2-3	30	2910	1.75	31	1/198	1/177	0.0028	8.6	23.0	0.070	A	0.9	0.7	1.00	0.38
U-2-4	30	3840	2.25	60	1/202	1/175	0.0034	6.7	29.6	0.089	A	0.8	1.1	1.12	0.49
U-2-5	30	2890	2.19	103	1/195	1/176	0.0057	6.8	28.8	0.090	A	1.4	1.7	0.69	0.76
U-2-6	30	2070	1.56	134	1/187	1/176	0.0042	9.6	20.5	0.067	A	1.1	1.0	0.90	0.62
U-2-7	30	1330	1.41	175	1/183	1/177	0.0076	10.6	18.6	0.061	A	1.6	1.3	0.60	0.94
U-2-8	30	750	0.89	240	1/183	1/179	0.0060	16.9	11.7	0.039	A	3.3	2.0	0.29	2.20
U-3-1	30	1330	1.39	0(390)	1/205	1/202	0.0065	10.8	18.3	0.054	A	3.6	2.5	0.26	1.80
U-3-2	30	2030	1.76	19(409)	1/207	1/198	0.0056	8.5	23.2	0.068	A	3.5	2.3	0.27	1.31
U-3-3	30	2910	2.09	43(433)	1/196	1/200	0.0049	7.2	27.5	0.085	A	2.9	1.8	0.32	0.86
U-3-4	30	3840	2.66	101(491)	1/213	1/188	0.0053	5.6	35.0	0.100	N	-	-	-	-
U-3-5	30	2890	2.18	187(577)	1/233	1/193	0.0047	6.9	28.7	0.074	A	1.5	0.8	0.63	0.37
U-3-6	30	2070	1.71	250(640)	1/203	1/199	0.0051	8.8	22.5	0.067	A	2.2	1.1	0.43	0.64
U-3-7	30	1330	1.40	331(721)	1/213	1/209	0.0064	10.7	18.4	0.052	A	2.6	1.1	0.36	0.79

as the initial bed configuration of the unsteady flow experiment. Duration time of run U-3 is 331 minutes and the time dependence of depth in run U-3 is expressed by Equation (2) and is shown in Figure 3. Equation (2) is the exactly same as Equation (1) when the water depth is larger than 1.5cm.

$$D_0 = \frac{2}{3}\left[\frac{\delta_f\left(\tau+\alpha_f'\right)^2}{\left(\tau+\alpha_f''\right)^2+\beta_f'}-\gamma_f\right]^{\frac{3}{2}} \qquad (2)$$

where $\alpha_f' = 0.839$, $\alpha_f'' = 0.060$ and $\beta_f' = 0.292$.

The water level and the riverbed height were measured in each case. The length of observed reach was 8.1m, between sections 2670cm and 3480cm downstream from the upper end of the laboratory flume in each experiment. The transverse measurements were at an interval of 5mm. The longitudinal measurements were at an interval of 30cm. Although the accuracy of each sandbar geometry might have deteriorated, the bed was measured at intervals of 30cm in the vertical section direction, in order to grasp the general bed geometry. The hydraulic quantities and bed form data of each unsteady flow experiment are summarized in Table 2. Measured water level in unsteady flow is slightly lower than the initially expected water level given by Equations (1) and (2).

The relationship between the change of depth with time and the alternate bar development process are shown in Figures 4 and 5. To clarify the influence of unsteady flow on the bar formation, results of steady flow experiments at

the times when the water depth of unsteady flow equaled those under steady flow are also plotted in these figures.

The alternate bar heights of runs U-1 and U-2 increase at a almost constant rate over time at the early stage, after which they either decrease or become constant and start increasing again. The alternate bars were present in run U-1 even in hydraulic conditions for which alternate bars were not generated under steady flow. The bar height decreased only slightly after the water level reached its peak. The sand bars started propagating again 270 minutes after the beginning of the experiments. At the final stage of the hydrograph, the bar height reached the same height as the fully developed bars in the steady flow experiments. Flood duration of run U-2 is one half of run U-1. The trend of bar development was approximately the same as in run U-1. However, the ratio of the time in flood duration to the time of lag between peak water depth and peak bar height was greater in run U-2 than in run U-1. Furthermore, the bar height reduction in run U-2 after the water level reached its peak exceeded that in run U-1. The bar height was less than that in the steady flow experiment.

The wavelength in run U-1 became the same as in the steady flow experiment after 60 minutes after the start of water flow. In run U-1, the wavelength was roughly constant until 350 minutes after the start of water flow, even during the period of hydraulic condition in which bars did not develop. After that, the wavelength increased to that in the steady flow experiment. In run U-2, the hydraulic conditions changed so that bars did not form during the bar development. Then the wavelength became shorter than in the steady flow experiment. When the bar height started to increase, the wavelength also started to grow, and it finally reached the same wavelength as the steady flow experiment.

On the other hand in run U-3, alternate bars disappeared at the term of peak water depth stage in which the hydraulic conditions were almost the same as that the alternate bars remained in run U-1.

LINEAR STABILITY ANALYSIS UNDER UNSTEADY FLOW CONDITION (9)

Basic Equations

The dimensionless depth-averaged St. Venant equations and the continuity equations are used for the incompressible flow and for the bed load in a straight channel.

$$\sigma\frac{\partial U}{\partial \tau}+U\frac{\partial U}{\partial x}+V\frac{\partial U}{\partial y}+\frac{\partial H}{\partial x}+\beta_B\frac{\tau_x}{D}=0 \tag{3}$$

$$\sigma\frac{\partial V}{\partial \tau}+U\frac{\partial V}{\partial x}+V\frac{\partial V}{\partial y}+\frac{\partial H}{\partial y}+\beta_B\frac{\tau_y}{D}=0 \tag{4}$$

$$\sigma\frac{\partial D}{\partial \tau}+\frac{\partial (UD)}{\partial x}+\frac{\partial (VD)}{\partial y}=0 \tag{5}$$

$$\frac{\partial\left(\overline{F}_B{}^2H-D\right)}{\partial t}+Q_B\left(\frac{\partial Q_{bx}}{\partial x}+\frac{\partial Q_{by}}{\partial y}\right)=0 \tag{6}$$

In Equations (3)-(6), the following scalings were used:

$$(U,\ V)=\frac{(\tilde{U},\ \tilde{V})}{\tilde{U}_B}\ ,\qquad D=\frac{\tilde{D}}{\tilde{D}_B}\ ,\qquad H=\frac{\tilde{H}}{F_B{}^2\tilde{D}_B}\ ,\qquad (Q_{bx},\ Q_{by})=\frac{(\tilde{Q}_{bx},\ \tilde{Q}_{by})}{\left(\Delta\tilde{g}\tilde{d}_s^{\,3}\right)^{\frac{1}{2}}}\ ,$$

$$(\tau_x,\ \tau_y)=\frac{(\tilde{\tau}_x,\ \tilde{\tau}_y)}{\tilde{\rho}\tilde{U}_B^{\,2}}\ ,\qquad (x,\ y)=\frac{(\tilde{x},\ \tilde{y})}{\tilde{B}}\ ,\qquad (\tau,\ t)=\left(\tilde{\sigma}\tilde{t},\frac{\tilde{U}_B}{\tilde{B}}\tilde{t}\right)$$

where $\tilde{x}$ and $\tilde{y}$ are coordinates in the longitudinal and the transverse directions, respectively, $\tilde{U}$ and $\tilde{V}$ are the flow velocity components along the $\tilde{x}$ and $\tilde{y}$ axes, respectively, $\tilde{\tau}_x$ and $\tilde{\tau}_y$ are the bed shear stresses along the $\tilde{x}$ and $\tilde{y}$ axes, respectively, $\tilde{\rho}$ is the density of water, $\tilde{g}$ is the acceleration of gravity, $\tilde{H}$ is the water level and $\tilde{D}$ is the water depth. In Equation (6), $\tilde{Q}_{bx}$ and $\tilde{Q}_{by}$ are the bed load transport in $\tilde{x}$ and $\tilde{y}$ directions, respectively. It is often observed that the time scale of bed formation is much greater than the response time of flow to bed forms. Therefore, the time variations of flow by the flood wave and sand wave are normalized by $1/\tilde{\sigma}$ and $\tilde{B}/\tilde{U}_B$, respectively in which $\tilde{B}$ is half of channel width and $\tilde{U}_B$ is the base flow velocity. The basic unit of $1/\tilde{\sigma}$ and $\tilde{B}/\tilde{U}_B$ is day and minute respectively. Moreover the following relevant dimensionless parameters arise:

$$\beta_B=\frac{\tilde{B}}{\tilde{D}_B}\ ,\qquad \sigma=\frac{\tilde{\sigma}\tilde{B}}{\tilde{U}_B}\ ,\qquad \Delta=\frac{\tilde{\rho}_s-\tilde{\rho}}{\tilde{\rho}}\ ,\qquad F_B=\frac{\tilde{U}_B}{\left(\tilde{g}\tilde{D}_B\right)^{1/2}}\ ,\qquad Q_B=\frac{\left(\Delta\tilde{g}\tilde{d}_s^{\,3}\right)^{1/2}}{(1-P)\tilde{U}_B\tilde{D}_B}$$

where $\tilde{H}_B$ and $\tilde{D}_B$ are the water level and water depth of base flow respectively, P is the porosity of bed sediments and $\tilde{\rho}_s$ is the density of sediment. σ is a small parameter because units of $1/\tilde{\sigma}$ and $\tilde{B}/\tilde{U}_B$ are day and minute (or hour) respectively.

The depth averaged flow velocity and sediment fluxes in the transverse direction are set to zero at the channel sidewalls as the boundary conditions

$$(V,\ Q_{by})=0\quad ;\quad y=\pm 1 \tag{7}$$

Sediment transport in the longitudinal and transverse directions is expressed, respectively, as

$$(Q_{bx},Q_{by})=\phi(\cos\delta,\sin\delta)$$

using the bed load function ϕ. In the above equation, δ is the deviation angle of the direction of flow from sediment transport direction, given by:

$$\sin\delta=V\left(U^2+V^2\right)^{-1/2}-\frac{r}{\beta_B\vartheta^{1/2}}\frac{\partial\left(F_B^{\,2}H-D\right)}{\partial y}\ ,\qquad \cos\delta=\left(1-\sin^2\delta\right)^{\frac{1}{2}}$$

in which r is a constant (=0.3) and ϑ is expressed as

$$\vartheta=\frac{F_B^{\,2}}{\Delta d_{sB}}\left(\tau_x^{\,2}+\tau_y^{\,2}\right)^{\frac{1}{2}}$$

where $d_{sB}=\tilde{d}_s/\tilde{D}_B$.

Linearization

In the context of a linear perturbation expansion, a flood wave itself was selected as the time-variable basic state to which a perturbation quantity due to sand bars is superimposed.

$$(U,V,H,D)=(U_0(t),0,H_0(t),D_0(t))+\varepsilon[U_1(x,y,t),V_1(x,y,t),H_1(x,y,t),D_1(x,y,t)]$$

where U_0, V_0, H_0 and D_0 are the functions of time t only, and do not depend on x or y.

Furthermore ϑ, τ_x and τ_y are set as

$$\vartheta=\vartheta_0(1+\varepsilon\vartheta_1), \qquad \tau_x=\tau_{x0}+\varepsilon\tau_{x1}, \qquad \tau_y=\varepsilon\tau_{y1}$$

in which ε is a parameter of perturbation.

In actual rivers, the wavelength of alternate bars at the time of a flood is much smaller than a flood wavelength. It can be considered that the basic state does not change along the longitudinal axis in short reach having a few bars. The basic wave depth and the associated flow velocity then only vary on the time scale of the flood wave while the slope of water level does not change in time.

The perturbation of the friction coefficient $C_f\left(=\tilde{U}_*^2/\tilde{U}^2, \tilde{U}_*;\text{shear velocity}\right)$ and of the bed load function ϕ are obtained by recalling their dependence on the Shields parameter and on the water depth. We then write:

$$\begin{aligned}(\phi,C_f)&=f(\vartheta,D)\\&=(\phi_0,C_{f0})\{1+\varepsilon[(\Phi_T,C_T)\vartheta_1+(\Phi_D,C_D)D_1]\}\end{aligned}$$

where

$$\Phi_D=\frac{D_0}{\phi_0}\frac{\partial\phi}{\partial D}\bigg|_{D=D_0} \qquad \Phi_T=\frac{\vartheta_0}{\phi_0}\frac{\partial\phi}{\partial\vartheta}\bigg|_{\vartheta=\vartheta_0} \qquad C_T=\frac{\vartheta_0}{C_{f0}}\frac{\partial c_f}{\partial\vartheta}\bigg|_{\vartheta=\vartheta_0}, \qquad C_D=\frac{1}{C_{f0}}\frac{\partial c_f}{\partial D}\bigg|_{D=D_0}$$

The initial condition for water-surface slope is set as I_{wB}, and the following equation is derived:

$$U_0=KD_0^{\frac{1}{2}} \tag{8}$$

where

$$K=\left[\frac{I_{wB}}{C_{f0}F_B^{\,2}}\right]^{\frac{1}{2}}$$

Differential equations at order ε^1 were obtained as follows:

$$U_0\frac{\partial U_1}{\partial x}+\frac{\partial H_1}{\partial x}+\frac{\beta_B}{1-C_T}\frac{U_0}{D_0}\left[2U_1+\frac{U_0}{D_0}\left(D_0C_D-1+C_T\right)D_1\right]=0 \tag{9}$$

$$U_0\frac{\partial V_1}{\partial x}+\frac{\partial H_1}{\partial y}+\beta_B c_{f0}\frac{U_0}{D_0}V_1=0 \tag{10}$$

$$D_0\frac{\partial U_1}{\partial x}+D_0\frac{\partial V_1}{\partial y}+U_0\frac{\partial D_1}{\partial x}=0 \tag{11}$$

$$\frac{\partial\left(F_B{}^2H_1-D_1\right)}{\partial t}+Q_B\phi_0\left[\frac{2\Phi_T}{1-C_T}\frac{1}{U_0}\frac{\partial U_1}{\partial x}+\left(\frac{C_D}{1-C_T}\Phi_T+\Phi_D\right)\frac{\partial D_1}{\partial x}+\frac{1}{U_0}\frac{\partial V_1}{\partial y}-\frac{r}{\beta_B\vartheta_0^{\frac{1}{2}}}\left(F_B{}^2\frac{\partial^2H_1}{\partial y^2}-\frac{\partial^2D_1}{\partial y^2}\right)\right]=0 \tag{12}$$

Growth rate of alternate bars

Linear perturbations (U_1,V_1,H_1,D_1) can be expressed by Equation (13) for alternate bar formation which automatically satisfies the boundary conditions.

$$\left(U_1,V_1\,H_1,D_1\right)=\left(\hat{U}_1S_1,\hat{V}_1C_1,\hat{H}_1S_1,\hat{D}_1S_1\right)E_1+c.c. \tag{13}$$

where

$$S_1=\sin\left(\frac{\pi}{2}y\right)\quad,\qquad C_1=\cos\left(\frac{\pi}{2}y\right)\quad,\qquad E_1=\exp\left[i\lambda\left(x-\omega x\right)\right]\quad,$$

i is the imaginary unit, $c.c.$ denotes the complex conjugates number and ω represents dimensionless bar angular frequency.

$\hat{U}_1,\hat{V}_1$ and $\hat{H}_1$ are expressed by Equations (14) as functions of $\hat{D}_1$, using Equations (9) to (11).

$$\left\{\hat{U}_1,\hat{V}_1,\hat{H}_1\right\}=\left\{f_U,f_V,f_H\right\}\hat{D}_1 \tag{14}$$

in which

$$f_U=-\frac{iK\left(-4ia_1\lambda^2+a_2\pi^2+a_3\right)}{\left(a_1a_4+ia_3\right)D_0^{\frac{1}{2}}}\quad,\qquad f_V=\frac{2K\pi\lambda\left(a_2+ia_1\right)}{\left(a_1a_4+ia_3\right)D_0^{\frac{1}{2}}}\quad,\qquad f_H=-\frac{4K^2\lambda\left(\beta_Bc_{f0}+i\lambda D_0\right)\left(a_2+ia_1\right)}{\left(a_1a_4+ia_3\right)D_0}\quad,$$

$$a_1=\left(C_T-1\right)\lambda D_0\quad,\qquad a_2=\beta_Bc_{f0}\left(-3+C_T+C_DD_0\right)\quad,\qquad a_3=2\beta_Bc_{f0}\left\{\pi^2-2\left(C_T-1\right)\lambda^2\right\}\quad,\qquad a_4=\pi^2+4\lambda^2$$

We finally obtain Equation (15), substituting Equation (14) into Equation (12).

$$\frac{\partial\hat{D}_1}{\partial t}+\mathbf{G}\left(d_{sB},\beta_B,\vartheta_B,D_0,\lambda\right)\hat{D}_1=0 \tag{15}$$

where the complex coefficient $\mathbf{G}\left(d_{sB},\beta_B,\vartheta_B,D_0,\lambda\right)$ is expressed by

$$\mathbf{G}(d_{sB},\beta_B,\vartheta_B,D_0,\lambda)=\frac{F_B^{\,2}}{F_B^{\,2}f_H-1}\frac{\partial f_H}{\partial t}+$$
$$\frac{Q_B\phi_0}{F_B^{\,2}f_H-1}\left[\frac{i\lambda}{1-C_T}\left(\frac{2}{K}\Phi_T f_U D_0^{-\frac{1}{2}}+C_D\Phi_T+\Phi_D(1-C_T)\right)-\frac{1}{2}\pi\left\{\frac{1}{K}f_V D_0^{-\frac{1}{2}}-\frac{1}{2}\pi\frac{r}{\beta_B\vartheta_B^{\frac{1}{2}}}\left(F_B^{\,2}f_H-1\right)\right\}\right] \tag{16}$$

Equation (16) controls the time evolution of the perturbation of flow depth due to the presence of alternate bars in a linear context. Equation (16) is solved as Equation (17), when $\mathbf{G}(d_{sB},\beta_B,\vartheta_B,D_0,\lambda)$ is independent of t.

$$\hat{D}_1=\zeta\exp[-\mathbf{G}t] \tag{17}$$

in which ζ is a constant of integration. The growth rate of perturbation under steady flow Ω_S is expressed by real part of $-\mathbf{G}$. Under unsteady flow conditions, D_0 and $\mathbf{G}(d_{sB},\beta_B,\vartheta_B,D_0,\lambda)$ are functions of t. Therefore, the solution of Equation (15) becomes Equation (18).

$$\hat{D}_1=\zeta\exp\left[-\int_{t_0}^{t}\mathbf{G}(t')dt'\right] \tag{18}$$

The real part of the term in square brackets of Equation (18) is the amplification factor Ω_U of alternate bars.

$$\Omega_S=-\mathbf{G}\quad,\qquad \Omega_U=-\int_{t_0}^{t}\mathbf{G}(t')dt'$$

Equation (18) indicates that the growth of perturbation is integrated with the instantaneous growth rate from the beginning of the hydrograph. When $-\mathbf{G}$ is positive, alternate bars grow; when the value is negative, the bars are damped.

The growth rate of alternate bars for any wave number λ is obtained by providing the suitable functions for friction coefficient and bed load function and given values of $d_{sB},\beta_B,\vartheta_B$ and D_0 which is a hydrograph. The wavelength λ_m, corresponding to the maximum growth rate $\Omega_{S\max}$ or $\Omega_{U\max}$, is selected by the instability process and should not be significantly modified by nonlinear effects as suggested by Colombini et al. (1). The amplitude of alternate bars Z_{bthe} is given by Equation (19).

$$\begin{aligned}Z_{bthe}&=\varepsilon\left(F_B^{\,2}f_H-1\right)\hat{D}_1\\&=\varepsilon\zeta\left(F_B^{\,2}f_H-1\right)\exp\left[-\int_{t_0}^{t}\mathbf{G}(t')dt'\right]\\&=\varepsilon\zeta Z_{b1}\end{aligned} \tag{19}$$

COMPARISON BETWEEN EXPERIMENTAL RESULTS AND THEORETICAL RESULTS

In order to verify the effectiveness of linear stability analysis under unsteady flow conditions, operational comparisons are made between the experiments and model results.

To calculate the model, the friction coefficient C_f is given by Equation (20) which has been obtained from the

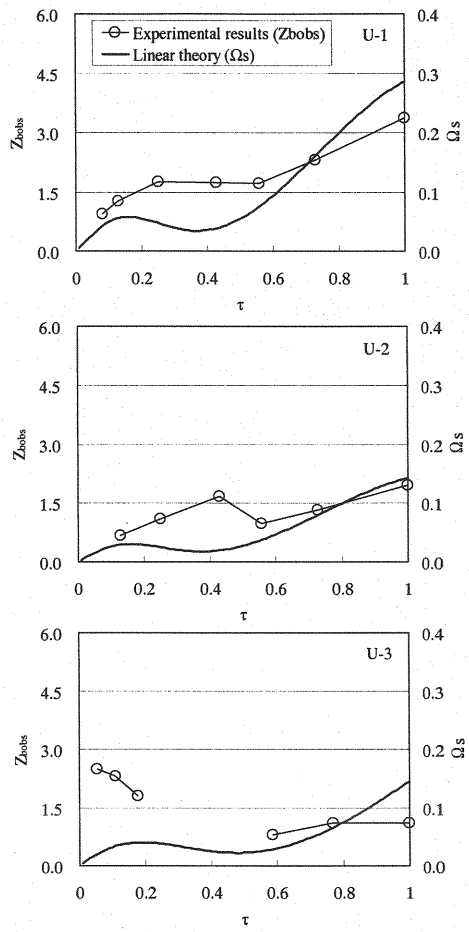

Figure 6 Comparison between the time integrated growth rates and the experimental bar heights

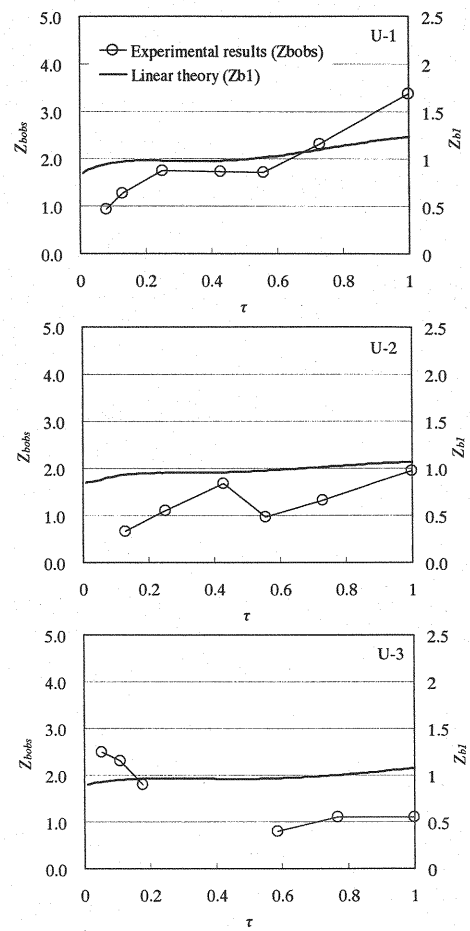

Figure 7 Comparison between the theoretical results and the experimental results

steady flow experiments.

$$C_f = 0.0113\vartheta_0^{0.069} \tag{20}$$

The bed load function ϕ proposed by Van Rijn (7) is used in the model.

$$\phi = 0.053\left(\frac{\vartheta' - \vartheta_c}{\vartheta_c}\right)^{2.1}\left(\frac{\tilde{\nu}^2}{\Delta\tilde{g}\tilde{d}_s^{\,3}}\right)^{0.1} \tag{21}$$

where ϑ' = the effective Shields parameter and $\tilde{\nu}$ = the coefficient of viscosity.

In general, the results of linear stability analysis of alternate bars under steady flow condition are used for a criterion of bar formation and not for estimation of bar height, because the development of bars is a nonlinear phenomenon. Figure 6 shows the comparison between Z_{bobs} and the time integrated growth rate Ω_u of the unsteady flow theory. The time integrated growth rate is positive in hydraulic conditions where alternate bars are not

generated under steady flow conditions. The time integrated bar growth rate predicted by the theory under unsteady flow has the same tendency as the measured values of bar height in all cases without beginning stage of U-3. It is anticipated that Z_{b1} in Equation (19) can express the experimental results. Figure 7 shows the comparison between the time dependence of Z_{b1} and Z_{bobs}. The change of Z_{b1} over time is a small compare with Z_{bobs}. In general, the bar height is dependent on the sediment discharge rate. As the amount of sediment discharge was not measured in the experiments, the coefficient of bed load function was adjusted so that the results of linear stability analysis became almost same values. The adjusted bed load function is expressed as Equation (22). It is necessary to check the validity of increasing the coefficient 5 times and the adaptability of the bed load function under unsteady flow conditions, in future.

$$\phi = 0.265\left(\frac{\vartheta'-\vartheta_c}{\vartheta_c}\right)^{2.1}\left(\frac{\tilde{\nu}^2}{\Delta\tilde{g}\tilde{d}_s^{\,3}}\right)^{0.1} \qquad (22)$$

The results of linear stability analysis used Equation (22) instead of Equation (21) are shown in Figure 8. In runs U-1 and U-2, Z_{b1} agrees well with Z_{bobs} when $\varepsilon\xi = 1$. In the beginning stage of run U-3, Z_{b1} does not agree with Z_{bobs}. The influence of initial bed configuration to the bar generation process cannot be neglected. This is a subject for future study.

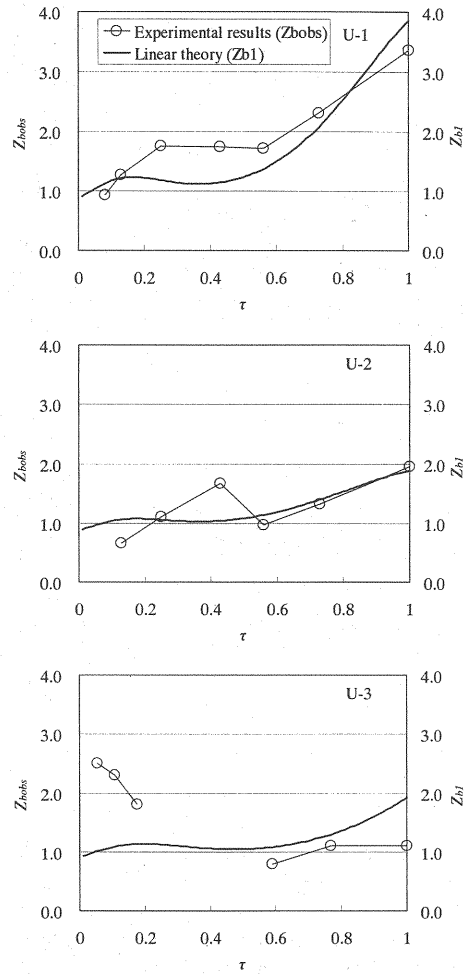

Figure 8 Comparison between the handled theoretical results and the experimental bar heights

The reasons why there was a good agreement between the results of linear stability analysis under unsteady flow conditions and the experimental results were considered. The bar height of full development of alternate bars $\tilde{Z}_{be}$ is expressed as Equation (23) by Ikeda (4).

$$\frac{\tilde{Z}_{be}}{\tilde{D}} = 9.34\left(\frac{2\tilde{B}}{\tilde{d}_s}\right)^{-0.45}\exp\left\{2.53\ \mathrm{erf}\left[\frac{\log_{10}\left(2\tilde{B}/\tilde{D}\right)-1.22}{0.594}\right]\right\} \qquad (23)$$

Dimensionless bar height $Z_{be}(=\tilde{Z}_{be}/\tilde{D})$ is affected by water depth. The relationship between the time of full development of alternate bars $\tilde{T}_e$ and $\tilde{Z}_{be}$ is shown in Equation (24) by Fujita et al. (2).

$$\frac{\tilde{Z}_{be}}{\tilde{T}_e} = \frac{\sqrt{s\tilde{g}\tilde{d}_s^{\,3}}\,\phi}{6\tilde{B}} \qquad (24)$$

According to this equation, the bar development velocity is in proportion to ϕ. The bed material diameter and water surface gradient are constant in the experiments. Therefore, the bar generation process is affected by the change of water depth. It was found that the change in hydraulic conditions over time are in accordance with hydrograph activity on bar development as an external force. The ratio φ of the water level variation rate $\partial\tilde{D}_0/\partial\tilde{t}$ to the bar development rate $\partial\tilde{Z}_b/\partial\tilde{t}$ is investigated, where $\tilde{Z}_b$ = bar height. φ is expressed by Equation (25) using the results of linear stability analysis.

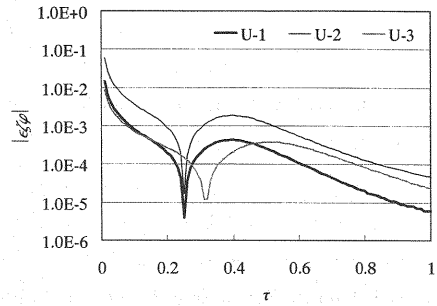

Figure 9 Time dependence of $|\varepsilon\zeta\varphi|$

$$\varphi = \frac{1}{\varepsilon\zeta}\frac{\partial D_0/\partial t}{\partial Z_{b1}/\partial t} \tag{25}$$

The theory is based on the assumption that $\partial\tilde{D}_0/\partial\tilde{t}$ is small comparing with $\partial\tilde{Z}_b/\partial\tilde{t}$. The changing of hydraulic condition over time cannot act on bar development as an external force, when $\partial\tilde{D}_0/\partial\tilde{t}$ is so smaller than $\partial\tilde{Z}_b/\partial\tilde{t}$. Therefore, when the bar development process is investigated, $|\varepsilon\zeta\varphi|$ must not be too large or too small. The changes of $|\varepsilon\zeta\varphi|$ over time are shown in Figure 9. This ratio changes dramatically over time. It was found that the suitable range of $|\varepsilon\zeta\varphi|$ for the theory is 0.0001 to 0.01 according to the comparison made between the experimental results and theoretical results. The order of $\varepsilon\zeta$ must be known to determine the applicability of this theory. In runs U-1 and U-2, Z_{b1} agrees well with Z_{bobs} when $\varepsilon\zeta = 1$. Then, the suitable range of $|\varphi|$ for the linear stability analysis under unsteady flow conditions becomes approximately 0.0001 to 0.01.

CONCLUSION

The hydraulic experiments were conducted in order to understand clearly the bar development process. On the basis of the experiments, it was learned that the bar generation process under unsteady flow conditions is different from under steady flow conditions. The hysterics of hydraulic conditions are a very important factor for bar generation. The wavelength and wave height of alternate bars differ significantly between unsteady and steady flow conditions and between the rising and falling stages of water levels due to the flood waves. The linear stability analysis is applied to development process of bars under unsteady flow conditions. The results of the theory agree well with the experimental results. The new parameter φ was introduced to express the applicability of the analysis. It was found that the linear stability analysis under unsteady flow conditions holds in the condition where $|\varphi|$ is 0.0001 to 0.01. However, the bar generation process is affected significantly by initial bed forms. Future studies of the effects of initial bed configurations on bar formation under unsteady flow conditions are needed.

ACKNOWLEDGEMENT

This study was funded by the Hokkaido Development Bureau, Ministry of Land, Infrastructure and Transport, Japanese government.

REFERENCES

1. Colombini, M., G. Seminara and M. Tubino : Finite amplitude alternate bars, Journal of Fluid Mechanics, Vol.181, pp.213-232, 1987.
2. Fujita, Y., Y. Muramoto and S. Horiike : Study on process of development of alternate bars, Disaster Prevention Research Institute Bull., Kyoto University, Vol.24, B-2, 1981. (in Japanese)
3. Hasegawa, K : Analysis on bed changes under unsteady flow with suspended sediments, Hokkaido Development Bureau sponsored research, 1998. (in Japanese)
4. Ikeda, S. : Wavelength and height of single row alternate bars, Proceedings of the 27th Japanese Conference on Hydraulics of JSCE, pp.689-695, 1983. (in Japanese)
5. Miwa, H., K. Ikeda and K. Tani : Growth and transformation process of alternate bars under the Sinusoidal-wave flood condition, Proceedings of the 55th Annual Conference of JSCE, pp.540-541, 2000. (in Japanese)
6. Tubino, M. : Growth of alternate bars in unsteady flow, Water Resources Research, Vol.27, No.1, pp.37-52, 1991.
7. Van Rijn, L. C. : Sediment transport, part I: bed load transport, Journal of Hydraulic Engineering, Vol.110, No.10, ASCE, pp.1431-1456, 1984.
8. Watanabe, Y. and M. Tubino : Influence of bed load and suspended load on alternate bar, Proceedings of Hydraulic Engineering Vol.36, JSCE, pp. 7-13, 1992. (in Japanese)
9. Watanabe, Y., M. Tubino, G. Zolezzi and K. Hoshi : Behavior of alternate bars under unsteady flow conditions, 2nd IAHR Symposium on River, Coastal and Estuarine Morphodynamics, pp.673-682, 2001.
10. Watanabe, Y., K. Sato and F. Oyama : Experimental study on bar formations under unsteady flow conditions, International Conference on Fluvial Hydraulics, River Flow 2002, 2002.

APPENDIX - NOTATION

The following symbols are used in this paper:

a_1 = $(C_T - 1)\lambda D_0$;

a_2 = $\beta_B C_{f0}(-3 + C_T + C_D D_0)$;

a_3 = $2\beta_B C_{f0}\left[\pi^2 - 2(C_T - 1)\lambda^2\right]$;

a_4 = $\pi^2 + 4\lambda^2$;

$\tilde{B}$ = half of channel width;

c.c. = Complex conjugate;

C_f = Frictional coefficient;

C_D = $(1/C_{f0})(\partial C_f / \partial D)\big|_{D=D_0}$;

C_T = $\left(\vartheta_0/C_{f0}\right)\left(\partial C_f/\partial\vartheta\right)\big|_{\vartheta=\vartheta_0}$;

C_1 = $\cos(\pi y/2)$;

d_s = Dimensionless grain diameter ($=\tilde{d}_s/\tilde{D}$);

d_{sB} = $\tilde{d}_s/\tilde{D}_B$;

$\tilde{d}_s$ = Bed material diameter;

D = $\tilde{D}/\tilde{D}_B$;

D_0 = $\tilde{D}_0/\tilde{D}_B$;

D_1 = Perturbation of water depth due to sand wave;

$\tilde{D}$ = water depth;

$\tilde{D}_B$ = Initial water depth (depth of base flow);

$\tilde{D}_P$ = The maximum water depth;

$\tilde{D}_0$ = Water depth of flood wave;

$\hat{D}_1$ = Amplitude of Perturbation D_1;

E_1 = $\exp(i\lambda x)$;

F_B = $\tilde{U}_B/\left(\tilde{g}\tilde{D}_B\right)^{1/2}$;

f_H = $-4K^2\lambda\left(\beta_B C_{f0}+i\lambda D_0\right)\left(a_2+ia_1\right)/\left[\left(a_1a_4+ia_3\right)D_0\right]$;

f_U = $-iK\left(-4ia_1\lambda^2+a_2\pi^2+a_3\right)/\left[\left(a_1a_4+ia_3\right)D_0^{1/2}\right]$;

f_V = $2K\pi\lambda\left(a_2+ia_1\right)/\left[\left(a_1a_4+ia_3\right)D_0^{1/2}\right]$;

$\tilde{g}$ = Acceleration of gravity;

G = Instantaneous growth rate of perturbation;

H = $\tilde{H}/\left(F_B{}^2\tilde{D}_B\right)$;

H_1 = Perturbation of water elevation due to sand wave;

H_0 = Dimensionless water elevation at basic state;

$\tilde{H}$ = Water elevation;

$\tilde{H}_B$ = Water elevation of base flow;

$\hat{H}_1$ = Amplitude of Perturbation H_1;

i = Imaginary unit;

I_b = Bed slope;

I_w = Water surface gradient;

I_{wB} = Initial condition for water surface slope (water surface gradient of basic flow);

K = $\left[I_{wB}/\left(C_{f0}F_B^{\ 2}\right)\right]^{1/2}$;

$\tilde{L}_b$ = Bar wave length;

P = Porosity of sediments;

Q_{bx} = $\tilde{Q}_{bx}/\left(\Delta\tilde{g}\tilde{d}_s^{\ 3}\right)^{1/2}$;

Q_{by} = $\tilde{Q}_{by}/\left(\Delta\tilde{g}\tilde{d}_s^{\ 3}\right)^{1/2}$;

$\tilde{Q}$ = Discharge;

$\tilde{Q}_{bx}$ = Bed load transport in $\tilde{x}$ direction;

$\tilde{Q}_{by}$ = Bed load transport in $\tilde{y}$ direction;

r = Constant;

S_1 = $\sin(\pi y/2)$;

t = $\tilde{t}/\left(\tilde{B}/\tilde{U}_B\right)$;

$\tilde{t}$ = Time;

$\tilde{T}$ = Elapsed time of flow;

$\tilde{T}_e$ = Fully development time of alternate bar;

U = $\tilde{U}/\tilde{U}_B$;

U_0 = Dimensionless flow velocity in $\tilde{x}$ direction at basic state;

U_1 = Perturbation of flow velocity in $\tilde{x}$ direction due to sand wave;

$\tilde{U}$ = Flow velocity component along the $\tilde{x}$ direction;

$\tilde{U}_B$ = Velocity of base flow;

$\hat{U}_1$ = Amplitude of Perturbation U_1;

V = $\tilde{V}/\tilde{U}_B$;

V_0 = Dimensionless flow velocity in $\tilde{y}$ direction at basic state;

V_1 = Perturbation of flow velocity in $\tilde{y}$ direction due to sand wave;

$\tilde{V}$ = Flow velocity component along the $\tilde{y}$ direction;

$\hat{V}_1$ = Amplitude of Perturbation V_1;

x = $\tilde{x}/\tilde{B}$;

$\tilde{x}$ = Longitudinal axes of coordinate;

y = $\tilde{y}/\tilde{B}$;

$\tilde{y}$ = Transverse axes of coordinate;

Z_{bobs} = $\tilde{Z}_{bobs}/\tilde{D}$;

Z_{bthe} = Dimensionless bar height calculated by the linear stability analysis;

Z_{b1} = Perturbation quantity of channel bed;

$\tilde{Z}_b$ = Bar height;

$\tilde{Z}_{be}$ = Fully developed bar height;

$\tilde{Z}_{bobs}$ = Experimental result of bar height;

α_f = Parameter of hydrograph;

$\alpha_f{}'$ = Parameter of hydrograph;

$\alpha_f{}''$ = Parameter of hydrograph;

β = Channel width depth ratio ($= \tilde{B}/\tilde{D}$);

β_f = Parameter of hydrograph;

$\beta_f{}'$ = Parameter of hydrograph;

γ_f = Parameter of hydrograph;

δ = Deviation angle between the direction of flow and sediment transport direction;

δ_f = Parameter of hydrograph;

ε = Parameter of perturbation;

ζ = Constant of integration;

ϑ = Shields parameter;

ϑ_0 = Shields parameter at basic state;

ϑ_1 = Perturbation of Shields parameter due to sand wave;

ϑ' = Effective Shields parameter;

λ = Bar wave number ($= 2\pi\tilde{B}/\tilde{L}_b$);

λ_m = Wave number of perturbation corresponding to the maximum growth rate of perturbation $\Omega_{S\max}$ or $\Omega_{U\max}$;

$\tilde{\nu}$ = Coefficient of viscosity;

$\tilde{\rho}$ = Density of water;

$\tilde{\rho}_s$ = Density of sediment;

$1/\tilde{\sigma}$ = Duration time of flood (hydrograph);

τ = $\tilde{t}/(1/\tilde{\sigma})$;

τ_x = $\tilde{\tau}_{sx}/\left(\tilde{\rho}\tilde{U}_B^{\,2}\right)$;

τ_{x0} = τ_x at basic state;

τ_{x1} = Perturbation of τ_x due to sand wave;

τ_y = $\tilde{\tau}_{sy}/\left(\tilde{\rho}\tilde{U}_B^{\,2}\right)$;

τ_{y1} = Perturbation of τ_y due to sand wave;

$\tilde{\tau}_x$ = Bed shear stress along the $\tilde{x}$ direction;

$\tilde{\tau}_y$ = Bed shear stress along the $\tilde{y}$ direction;

ϕ = Bed load function;

ϕ_0 = Bed load at basic state;

ϕ_1 = Perturbation of bed load due to sand wave;

Φ_D = $(D_0/\phi_0)(\partial\phi/\partial D)\big|_{D=D_0}$;

Φ_T = $(\vartheta_0/\phi_0)(\partial\phi/\partial\vartheta)\big|_{\vartheta=\vartheta_0}$;

φ = Ratio between the variation velocity of water elevation and the bar development velocity;

ω = Dimensionless bar angular frequency;

Ω_S = Growth rate of perturbation under steady flow condition;

$\Omega_{S\max}$ = Maximum growth rate of perturbation corresponding to various λ under steady flow condition;

Ω_U = Growth rate of perturbation under unsteady flow condition; and

$\Omega_{U\max}$ = Maximum growth rate of perturbation corresponding to various λ under unsteady flow condition.

(Received July 25, 2002 ; revised January 25, 2003)